ANL/MSD/FE-80-7

(1)

ANL/MSD/FE-80-7

27
1-19-81 5H

MASTER

DEVELOPMENT OF NONDESTRUCTIVE EVALUATION TECHNIQUES FOR HIGH-TEMPERATURE CERAMIC HEAT EXCHANGER COMPONENTS

Twelfth Quarterly Report, July—September 1980

ARGONNE NATIONAL LABORATORY

ARGONNE NATIONAL LABORATORY, ARGONNE, ILLINOIS

Prepared for the Office of Fossil Energy
U. S. DEPARTMENT OF ENERGY
under Contract W-31-109-Eng-38

DISCLAIMER

The facilities of Argonne National Laboratory are owned by the United States Government. Under the terms of a contract (W-31-109-Eng-38) among the U. S. Department of Energy, Argonne Universities Association and The University of Chicago, the University employs the staff and operates the Laboratory in accordance with policies and programs formulated, approved and reviewed by the Association.

MEMBERS OF ARGONNE UNIVERSITIES ASSOCIATION

The University of Arizona
Carnegie-Mellon University
Case Western Reserve University
The University of Chicago
University of Cincinnati
Illinois Institute of Technology
University of Illinois
Indiana University
The University of Iowa
Iowa State University
The University of Kansas
Kansas State University
Loyola University of Chicago
Marquette University
The University of Michigan
Michigan State University
University of Minnesota
University of Missouri
Northwestern University
University of Notre Dame
The Ohio State University
Ohio University
The Pennsylvania State University
Purdue University
Saint Louis University
Southern Illinois University
The University of Texas at Austin
Washington University
Wayne State University
The University of Wisconsin-Madison

Printed in the United States of America
Available from
National Technical Information Service
U. S. Department of Commerce
5285 Port Royal Road
Springfield, VA 22161

NTIS price codes
Printed copy: A03
Microfiche copy: A01

Distribution Category:
Coal Conversion and Utilization—
Materials and Components (UC-90h)

ANL/MSD/FE-80-7

ARGONNE NATIONAL LABORATORY
9700 South Cass Avenue
Argonne, Illinois 60439

DEVELOPMENT OF NONDESTRUCTIVE EVALUATION TECHNIQUES FOR HIGH-TEMPERATURE CERAMIC HEAT EXCHANGER COMPONENTS

Twelfth Quarterly Report
July—September 1980

Materials Science Division

October 1980

THIS PAGE

WAS INTENTIONALLY

LEFT BLANK

TABLE OF CONTENTS

LIST OF FIGURES

LIST OF FIGURES (continued)

LIST OF FIGURES (continued)

HIGHLIGHTS

Detection of electric-discharge machined notches in a silicon carbide tube by an ultrasonic bore-side probe under microcomputer control has been demonstrated. Use of the reflection mode has been shown to enhance the sensitivity of flaw detection with an acoustic microscope. In this configuration, the transducer and laser-scanned coverslip are both on the tube outer surface, eliminating the need to fill the tube with water. A conceptual design is presented for inspecting tubes up to seven feet long in both through-transmission and reflection-mode configurations. A comparison of NDE techniques for ceramic butt joints showed holographic interferometry to be generally better than dye-penetrant, radiographic, or ultrasonic techniques for characterizing a crack-like inner-wall defect. Pitch-catch and pulse-echo ultrasonic techniques also indicated the presence of an anomaly in the region identified as flawed via holography, while radiographic and penetrant-testing results were ambiguous.

DEVELOPMENT OF NONDESTRUCTIVE EVALUATION TECHNIQUES FOR HIGH-TEMPERATURE CERAMIC HEAT EXCHANGER COMPONENTS

Twelfth Quarterly Report
July-September 1980

D.S. Kupperman, M.J. Caines, and D. Yuhas*

I. INTRODUCTION

High-temperature ceramic heat-exchanger components are of particular interest because they are lighter than their metallic counterparts, have better high-temperature mechanical properties and good corrosion resistance, and can be fabricated from inexpensive and abundant elements. As a result, the use of these ceramics at temperatures > 1000°C (higher than metals can withstand) can lead to more efficient energy-conversion systems.

In recent years, significant progress has been made in the use of ceramics for structural applications. Silicon carbide (SiC), for example, is currently being used for heat-exchanger tubing because of its excellent thermal-shock resistance, low coefficient of expansion, high thermal conductivity, and strength at high temperature.

The reliable use of ceramics as structural components, however, requires effective failure prediction and thus effective flaw-detection capabilities. The flaws with the most deleterious effects on the lifetime of SiC components are cracks and porosity. Many fracture origins are adjacent to the surface,[1] indicating that surface cracks are an important cause of failure. The size of critical cracks leading to fracture can be related to microstructural features such as grain size, and can be relatively small (an order of magnitude or more smaller than in comparable metallic parts). For example, to assure high reliability of ceramic heat-exchanger tubes, an inspection technique must be capable of detecting defects of the order of 100 μm in size. Thus, nondestructive evaluation (NDE) techniques that are satisfactory for metals may not be for ceramics. Depending on the component of interest, it may be necessary to develop or advance conventional NDE techniques for ceramic applications. Currently, the techniques most widely employed by industry for ceramic NDE are x-radiography and fluorescent dye penetrant testing. However, efforts are under way at Argonne National Laboratory (ANL) and several other institutions to advance NDE techniques for structural ceramics. The techniques that have been studied outside ANL include high-frequency (> 50-MHz) ultrasonic testing,[2] microfocus x-radiography,[2] microwave NDE,[3] acoustic surface-wave testing,[4] photoacoustic microscopy,[5] acoustic emission detection,[6] and overload proof testing.[7]

The purpose of the present ceramic NDE program is to compare the effectiveness of several conventional and unconventional NDE techniques for flaw detection in specific high-temperature ceramic components. The investigation encompasses many NDE techniques, concentrating on those not under extensive evaluation at other institutions. The techniques under study at ANL have

*Sonoscan, Inc., Bensenville, IL.

included dye-enhanced radiography, acoustic microscopy, conventional ultrasonic testing, acoustic-emission detection, acoustic impact testing, holographic interferometry, infrared (IR) scanning, internal friction measurements, and overload proof testing. No single technique is expected to serve as a universal flaw-detection method; several techniques will be required to thoroughly assess ceramic components in a cost-effective way. After the investigation of many NDE techniques, one or more promising methods will be developed further for the specific ceramic components of interest. The current effort involves SiC heat-exchanger tubes; previous ceramic NDE efforts at ANL have involved silicon nitride gas-turbine rotors.[8]

The current report discusses recent results on inspection of SiC heat-exchanger tubing, including butt and overlap joints, by means of ultrasonic, IR, and holographic techniques.

II. COMPUTER-INTERFACED ULTRASONIC BORE-SIDE PROBE

One of the objectives of the present program is to develop a design for an ultrasonic bore-side probe to scan SiC tubes automatically under the control of a microcomputer. The system, described in detail in Ref. 9, consists of a Sonic Mark III pulser-receiver and 22-MHz Aerotech transducer propagating longitudinal waves normal to the tube wall. In the previous quarterly report,[10] a computer-interfaced version of the system was described and the sensitivity for detecting electric-discharge machined (EDM) notches was evaluated. Efforts during the present quarter were concerned with detection of flat-bottom holes by longitudinal waves, reproducibility of the positioning achieved with the axial drive mechanism, and computer-controlled scanning and detection of EDM notches.

Three flat-bottom holes were drilled in the outer wall of a SiC tube, as shown schematically in Fig. 1. The ability of the ultrasonic bore-side probe to detect the presence of these holes is indicated in Fig. 2. The large peak at the left side of each trace is the reflection from the water/tube interface at the inner surface of the tube. Multiple reflections beyond the hole echo can also be seen. Unfortunately, the interface and multiple-reflection echoes are rather wide and signals from flaws near the tube inner wall will be difficult to isolate. With the present system and a 3-mm wall thickness (0.5-μs transit time), the first mm of the tube wall will be virtually unexaminable with longitudinal waves. Thus, laminar-type defects (as simulated here by the flat-bottom holes) within the first mm of wall will have to be detected by shear waves in a pitch-catch mode or by a system having shorter pulses and higher frequency. A short pulse, 50-MHz transducer has been ordered from Panametrics and will be compared with the present one for effectiveness in detecting such flaws.

The results from Fig. 2 suggest that (a) laminar-type flaws $\sim$ 500 μm in diameter can be readily detected by the current system, and (b) the beam is focused so sharply owing to the curvature of the tube that under the right circumstances, 1-mm-dia and larger reflectors in the middle of the wall may reflect virtually all of the beam, significantly reducing the amplitude of multiple reflections from the backwall.

The stepping motor that drives the probe axially has 400 steps/in. of vertical travel; thus, each step or count of the motor moves the probe up or down by 64 μm (0.0025 in.). The system was checked to establish whether the axial position can be reproduced to within ∿ 100 μm. Figure 3 shows the traces obtained (a) at the position of the 1.5-mm-dia hole, (b) after the probe was lowered ∿ 13 mm, and (c) after the probe was returned to the original position. These movements are controlled by the microcomputer. As can be seen, the echo pattern obtained after the probe traversed 13 mm and returned is virtually the same as the original. Other tests with longer axial motions lead to the same conclusion: The system, as currently designed, can be returned to a location with an error of less than 100 μm.

A study was carried out to indicate the capability of the bore-side probe to detect an EDM notch while under complete microcomputer control. In this example, the probe was inserted into siliconized SiC tube J (Ref. 9) and moved over an axial range of 13 mm. The computer printout correctly indicated the location of a 500-μm-deep x 1250-μm-long EDM notch to within 0.25 mm. The printout is shown in Fig. 4. The mirror was rotating at a rate of 5 r/s. Flaw information was acquired after every 6° of angular displacement (about every 1.5 mm of circumferential travel), and an angular scan was taken in the axial direction every 312 μm (0.012 in.) or every 5 steps.

The computer output shown in Fig. 4 indicates flaw signals at axial positions 970 and 975 for the first scan, and positions 965 and 970 for the second scan. Maximum flaw amplitudes of 105 and 117 units (equivalent to an analog output of ∿ 0.25 V) are indicated in the two passes of the EDM notch. The threshold level was set at 100 amplitude units. The analog output of the ultrasonic pulser-receiver was set for a gate which would only transmit flaw signals for reflectors near the tube outer wall. The "stretched" mode was employed, which means that the notch signal is held for about 20 ms; thus, the 1.25-mm-long notch, which should only be detected at one angular position, was recorded at several angular positions. This assures that the notch will not be missed in a scan. The notch is seen at more than one axial position because the beam spans about 3 mm of axial length (about 50 axial positions). Maintaining a threshold level of about 0.25 V prevents the notch signal from being recorded at even more locations. Since the signals are not recorded continuously and the motor driving the mirror does not maintain a constant speed (the speed varies by ∿ 20%), the output data is not entirely reproducible. Improvements are planned to minimize these problems. Comments next to the computer printout provide more details regarding this computer program and test. Although this scan was slow (2 mm/s), in principle it could be carried out at a rate of 500 mm/s (20 in./s). Work is progressing on modifications of the system to allow for this more rapid inspection rate.

III. ACOUSTIC MICROSCOPY

Previous work has demonstrated the feasibility of through-wall inspection (with insonification from the inner to the outer surface) for cracks and other structural elastic inhomogeneities in short, water-filled SiC tube segments.[9] Additional methods employing reflection/refraction imaging, if successful, might be more attractive for long tubes since the entire tube would not have to

be submerged in a bath. In this section, tests of acoustic lenses fabricated at ANL are described, and the observations compared with results obtained without lenses. Studies of alternate reflection geometries are also discussed, and the results compared with those obtained previously. Finally, a conceptual design for testing seven-foot lengths of SiC tubing is presented.

A. Through-wall Imaging

1. Focusing Effects

Figure 5 is a schematic showing the refraction (focusing) of the sound field as it propagates from the inner to the outer surface of a SiC tube. (The actual situation is even more complicated than that shown in Fig. 5; incident sound mode converts at the inner surface, forming two foci, one for shear waves and one for longitudinal waves. In practice, the two sound fields overlap spatially.) Two features in the acoustic images may be attributed to the curved tube geometry: (1) The sound field is apertured by critical-angle considerations at the input surface, and (2) the focusing of the sound field by the tube wall leads to distortion in the images of buried flaws. This will influence the interpretation of flaw type as well as the estimation of flaw size. The upper drawing in Fig. 5 shows the incident plane wave brought to focus inside the tube wall. Three regions of the sound field should be considered: (a) above the focal zone, near the outer surface; (b) at the focal zone; and (c) below the focal zone, near the inner surface. For flaws in region (a), the images resemble those obtained from planar insonification. However, as flaws successively closer to the focal zone are detected, increasingly magnified images are obtained. At the focal zone, the projected image of a flaw may fill the entire field of view of the micrograph. For example, a flaw might be indicated by transformation of the entire field of view from light to dark. In region (c), the images will be inverted and magnified. Structures in the images arising from flaws in this zone possess the unique characteristic that as the tube is rotated in one direction, the structures move in the opposite direction.

An acoustic lens can be used to convert the incident plane wave into a cylindrically diverging wave and thus compensate for this focusing effect, as illustrated in Fig. 6. By matching the curvature of the sound field to the curvature of the tube inner wall, the critical-angle aperturing effect and complex image characteristics associated with the focused sound field can be eliminated. What we are doing is converting the cylindrical component imaging problem into the more familiar plane-wave imaging problem. The motivation for doing this is that a large body of data exists for flaw characterization in ceramics using planar insonification. The lens approach would permit us to take full advantage of this data base.

Diffusing lenses were fabricated from aluminum bar stock, which is easily machined and has a sufficiently clean acoustic structure to allow testing of the lens concept. The lenses were placed on top of a standard 30-MHz sound cell in the configuration shown in Fig. 6. The acoustic amplitude micrograph and interferogram in Fig. 7 illustrate the divergent sound field produced by an aluminum lens with a 10-mm radius of curvature. The speckle in the picture results from grain-boundary scattering in the lens. Although the curvature of the lens matches that of the inner surface of the tube,

the curvature of the sound field is not sufficient to fully compensate for the tube geometry owing to the large sonic velocity difference between aluminum and SiC.

The effect of the lens on the acoustic image of a tube segment is shown by a comparison of Figs. 8 (without lens) and 9 (with lens). In Fig. 9, the sound field is wider and the fringes are straighter; however, greater sound-field curvature (more diffusing of the beam) is still needed. Additionally, artifactual structure arises from grain structure in the aluminum, reverberation in the lens, and reverberation in the space between transducer and lens. All of these limitations can be overcome by better lens design, better material choice, and direct bonding of the peizoelectric element to the lens.

Other lenses made from glass and silicon nitride were fabricated at ANL and tested in a similar fashion to the aluminum lens. These materials were acoustically clean and therefore did not contribute to the signal; however, reverberation was a more serious problem because they were much thinner than the aluminum lens.

We conclude that the concept is viable but that appropriate lens design is essential to realize the desired results experimentally. Specific conclusions are as follows:

(a) The aluminum lens produced the expected result, i.e., flattening of the sound field.

(b) Reverberation of sound in the lens produced a significant amount of artifactual structure in the image, but this can be eliminated by careful design.

(c) Reverberation of sound in the space between the lens and the transducers also produced artifacts, but this can be eliminated by bonding the piezoelectric element directly to the lens.

2. Comparison of Axial and Circumferential Insonification

Through-wall insonification may utilize either an axial or circumferential geoemtry; these are shown schematically in Figs. 10 and 11, respectively. Both geometries produce bright-field acoustic images that are similar in size and general appearance to optical images. Images produced by axial insonification are characterized by a bright horizontal band $\sim$ 3 mm wide. In contrast, circumferential insonification produces images with a bright vertical band, as illustrated in Fig. 12, an acoustic amplitude micrograph of sintered SiC tube SRI (Ref. 9).

In general, imaging of flaws in the SiC tubes was relatively tolerant of the insonification angle (Fig. 5). However, visibility varied (particularly for outer-surface notches) as the flaw was rotated through the fixed sound field. This effect is illustrated in the series of micrographs shown in Fig. 13; these were taken in the vicinity of the same EDM notch shown in Fig. 12a, again with circumferential insonification. The notch is located at the right edge, center, and left edge of the sound field in Figs. 13a, b, and c, respectively. The notch is readily detected when positioned at

either edge of the sound field, but not when positioned in the middle. This effect is much more dramatically illustrated during real-time viewing on the monitor; the notch is visible "coming and going", but disappears when in the center of the field.

The explanation for these observations lies in the fact that as the notch is rotated, the propagation angle of the interrogating sound wave relative to the notch varies continuously. At some orientation the sound wave is exactly parallel to the notch axis and thus difficult to observe. Additionally, copious mode conversion at the notch makes this flaw type a strong radiator of acoustic energy, which in certain orientations will add to the incident beam and mask its presence. The latter statement is supported by the ability of the system to produce dark-field images. These can be obtained because the laser detection method is sensitive to the incident angle of sound impinging on the coverslip. Thus, dark-field images are produced by placing the notch in a region of the sound field that is not normally detected by the laser beam. Acoustic energy is scattered by the flaw into the angular-acceptance aperture of the laser scanner, as illustrated in Fig. 14. In this situation, the flaws (Fig. 15) appear bright because we are detecting the energy they have scattered. In the normal transmission mode (Figs. 12 and 13), the flaws are dark because we are detecting the energy they have removed from the interrogating beam.

B. Reflection Imaging

Axial and circumferential insonification geometries can also be used in the external mode, with both the transmitting transducer and the receiving scanning laser located outside the tube. Both methods are useful for flaw characterization, as demonstrated below.

1. Axial Insonification

From a standpoint of image quality, axial insonification appears to be superior to circumferential insonification for reflection imaging. With axial insonification, the sound is transmitted through the tube, reflected from the inner surface, and detected at the coverslip, as shown schematically in Fig. 16. Figures 17 through 19 show, respectively, a "clean" zone, a buried inclusion, and longitudinal outer-surface notches in tube SRI, all imaged by axial insonification.

2. Circumferential Insonification

Figure 20 illustrates the geometry for external circumferential insonification. Figures 21 and 22 schematically illustrate the propagation of shear waves and longitudinal waves in a SiC tube undergoing such insonification. Successful use of the technique requires a smooth tube surface. In practice, the axial positions of the tube and coverslip were fixed and the tube was rotated about its long axis. Empirically, we found that for a given circumferential location of the transducer, a transducer alignment could be found which produced a good image of the notches. The movements of the transducer holder were too imprecise to allow accurate measurement of the angles. However, the image quality could be easily reproduced and did not appear to require a

unique combination of transducer location and angulation. For precise location of buried flaws, both angles and working distance (separation between transducer and sample) need to be accurately measured.

Interpretation of the images produced by external circumferential insonification requires an understanding of the propagation paths followed by the sound. The sound reaching the coverslip appears to segment into three distinct fields; an interpretation of their origins is shown in Fig. 23, and Figs. 24 and 25 illustrate the characteristics of the three sound fields. Sound field #1 probably corresponds to that portion of the incident energy which passes through the tube wall, is reflected from the inner surface, and impinges on the coverslip. Sound field #2 appears as a bright vertical band directly to the right of sound field #1. It is not clear why sound field #2 appears as a well-defined unit; however, the large longitudinal notch in the tube appears as a dark zone (circled). The lack of shadowing, together with the invariant visibility and shape of the flaw indication as the flaw is rotated through the field, suggests that this bright zone results from specular reflection of sound from the outer surface of the tube (Fig. 23). Sound field #3, visible in Fig. 25, also results from the specular reflection of sound from the outer tube surface. Clearly, only sound field #1 will be of use in probing the interior of the sample.

Figure 26 shows an image of the large longitudinal EDM notch. The image was produced using circumferential insonification, with the notch in sound field #1. The width of the shadow indicates a steep propagation angle relative to the notch. This insonification method may be suited for measuring crack extension.

C. Conceptual Design for Inspection of Seven-foot Lengths of Tubing

In this and previous reports, it has been shown that ceramic heat-exchanger tubes can be characterized with the acoustic microscope. Complete characterization of flaws requires a dual operating frequency of 30 and 100 MHz. In particular, 100 MHz has shown the strongest potential for detailed analysis of inner-surface flaws by through-wall imaging, while 30 MHz is optimal for reflection imaging and for detecting outer-surface flaws. Reflection imaging offers an advantage in that the transducer assembly is outside the tube and nothing need be inserted. Also, we have observed substantial attenuation differences among the various samples tested, which may preclude the use of the 100-MHz system in some tube types.

The conceptual design described below is basically an extension of the system already employed to inspect short tube segments. The output of this system is simultaneously available in three forms: (1) CRT image in real time, (2) video print on thermal roll paper, and (3) output for direct computer interfacing. Of course, photographs of the CRT output are also available. Flaw characteristics and positions are stored in the memory for long-term follow-up of tube performance under service conditions. For purposes of discussion, the long-tube inspection system may be divided into the following components:

(1) Transducers.
(2) Through-wall transmission stage.
(3) Reflection stage.
(4) Tube-positioning apparatus.
(5) Detection system.

The detection system, a scanning laser acoustic microscope, has been discussed previously in this series of reports as well as in the open literature. The other elements of the system are described below.

1. Transducers

The piezoelectric elements used as ultrasonic transducers in acoustic microscopy can be rather delicate owing to their high operating frequency. Therefore, backings will be used to provide mechanical support. For use in microscopy, the transducers must have uniform output over the field of view. Each will be electrically matched to a 50-Ω line for optimum performance. It is particularly important to accomplish the matching near the piezoelectric element so that cable length variations do not affect the output. Transducers have been fabricated with a piezoelectric element and matching network in a small watertight housing that will fit inside the tube.[9] This is essential for through-transmission inspection; for reflection imaging, the size limitations on the transducer housing can be relaxed. The transducer for use inside the tube will also contain intergral spring-loaded bearings to guide it along the inner surface as the tube position is indexed. Both transducers will be embodied within an articulation mechanism to allow for some flexibility during inspection of specific defects.

2. Through-wall Transmission Stage

The techniques developed for inspection of short tube segments should be adaptable to long tubes. The acoustic microscope produces its images by scanning a laser beam over a plastic mirror (coverslip), which is in close proximity to the subject being visualized. The mirror surface, which has impressed upon it an optical phase replica of the acoustic image, acts as the receiving plane. For through-wall imaging, the source (transducer) is placed on the opposite side of the sample from the coverslip. In the case of a tube, the transducer is inserted within the tube bore, whereas the coverslip is on the outer surface. The acoustic energy must be coupled to the sample and coverslip with a fluid. This is accomplished by filling the tube with water. Caps on either end of the tube retain the water and provide ports for filling and emptying. The coverslip is acoustically coupled to the outer surface by a continuous but slow water stream dripping onto the tube in the vicinity of the coverslip. The water is retained by capillary action. Excess water is captured in a tray below and recycled to the coverslip.

The transducer housing is mounted on a gimble so that the transducer can be angulated both axially and circumferentially. This angle will be controlled externally; thus, circumferential insonification as well as axial insonification can be accomplished with a single transducer.

3. Reflection Stage

For reflection imaging, the transducer and coverslip will be located on the outer surface of the tube and coupled by means of a flowing stream of water, as shown in Fig. 27. No water need be placed inside the tube. The position and angle of the transducer with respect to the tube will determine the insonification technique, e.g., shear, longitudinal, or surface waves. Thus, it will be possible to change the imaging mode as needed to enhance and analyze different types of anomalies.

4. Tube-positioning Apparatus

In either stage configuration, the transducer and coverslip have to be adjusted with respect to the tube and to each other, and the tube then rotated and translated the field of view. The movement through the field of view will be helical during scanning, but also adjustable for pure rotation or pure translation. Since the tubes to be inspected can be up to 7 feet long, a system up to 14 feet long will be required. The apparatus will be constructed around a scanning laser acoustic microscope, which will be modified in a number of ways. For example, the laser scan will be capable of 90° rotation to make the vertical scan axis parallel to either the circumference or the long axis of the tube. This is necessary in order to achieve the axial and circumferential insonification geometries described earlier. Also, the field of view and laser spot size will be switchable for the dual 30/100-MHz frequencies.

Figure 28 shows the overall design for an acoustic microscope system for through-wall imaging of long tubes. For reflection imaging, the mechanism for filling the tube with water and sealing it, along with the rod for holding the transducer and matching network, would be replaced by the arrangement shown in Fig. 27. The advantages and disadvantages of through-wall and reflection imaging have been discussed. More experience with the two types of systems will be necessary to determine whether just one would be practical and adequate to obtain the flaw characterization desired.

IV. COMPARISON OF NDE TECHNIQUES FOR A CERAMIC BUTT JOINT

Previous reports[9,11] in this series discussed the detection of a subsurface crack-like flaw in a 150-μm-wide butt joint of an NC430 SiC tube (J6) by holographic interferometry. Figure 29 shows a micrograph of a ceramic joint (arrow) in a similar tube. The small grain size of the joint relative to the tube wall is evident. During the present quarter, tube J6 was examined by dye-penetrant, radiographic, and ultrasonic techniques to compare the effectiveness of these methods with that of holographic interferometry.

In the first test, the outer surface of tube J6 was exposed to a fluorescent dye penetrant. The results were somewhat ambiguous because of the irregular surface. A linear indication was seen in the outer surface of the joint in the region where the interferometry suggested an inner-surface crack, but the dye washed out very easily, suggesting that the indication was due to a slight step or mismatch in the joining of the tubes.

The tube was then radiographed, and again the results were ambiguous. No "crack-like" indication was seen; however, the entire joint appeared to have a lower density than the tube wall.

The ultrasonic testing did indicate an anomaly in the region where a flaw had been detected with holography. Figure 30 shows the experimental arrangement and results. Two 20-MHz contact transducers were employed in a pitch-catch configuration; the transducer pair was moved around the tube and the amplitude of the received signal was monitored. A weak signal indicates that something has interrupted the beam or the material attenuation has changed. The flaw seen by holographic interferometry appeared in the 0° position of region A, and indeed, the received ultrasonic signal (Fig. 30, lower right) was $\sim$ 6 dB lower in the 0° position than in any other area of the joint, and more than 6 dB lower than in regions B and C (the tube walls). The data in Fig. 30 show that the attenuation in the tube joint is less than that in the tube wall, although the radiographic results suggested that the joint has a relatively low density which would be expected to increase the attenuation. Characterizing the flaw by this method is, of course, very difficult.

The SiC tube was also interrogated by a single transducer, in a similar configuration to that of Fig. 30. Here, an echo from a defect would appear among other geometrical reflector signals. Figure 31 shows signals obtained at the 0° and 45° positions of the joint. At the 0° position, there is indeed an unidentified ultrasonic reflector. The echoes on both sides of the flaw signal are the result of the roughness and irregular geometry of this particular sample. At 45° and other positions around the tube, no flaw signals were observed. These results suggest that ultrasonic testing is a viable technique for examining butt joints in SiC tubes but that because of the irregular geometry, holographic interferometry may be more effective in characterizing the flaws. Future work will include ultrasonic testing from the bore side, as well as more extensive efforts employing acoustic microscopy and holography.

V. DESTRUCTIVE INSPECTION OF A CERAMIC OVERLAP JOINT

The previous quarterly report[10] presented IR pictures of an NC430 SiC tube containing an overlap joint made with Corning #0080 glass adhesive. This specimen was expected to have a poor bond. A cool spot was detected in the tube, indicating a localized region of good heat conduction (the heat flow in this case was from the OD to the ID). The remaining portion of the tube at this axial position showed poor heat conduction. The tube was sectioned at the level of the cool spot to determine the cause of the anomaly. Figure 32 shows the tube cross section. The bond is clearly better in the "cool" region (arrow) than elsewhere; thus, one might expect better heat transfer in this area, with a resultant anomaly in the IR image. While this example shows good bonding in a poorly bonded specimen, one can expect reciprocal results for poor bonding in an otherwise properly bonded tube. Tests will continue on tubes with properly bonded overlap joints as they become available.

VI. SUMMARY

Detection of an EDM notch in the outer surface of a SiC tube with an ultrasonic bore-side probe (22-MHz transducer) under microcomputer control has been demonstrated. Detection of laminar-type defects will require a normal-incidence longitudinal probe with a more highly damped, higher-frequency transducer.

Detection of EDM notches with the acoustic microscope in the dark-field imaging mode has been demonstrated for EDM notches as small as 125 μm deep x 250 μm long. Detection of outer-surface notches using reflection imaging, with both the transducer and the laser-scanned coverslip on the outer surface of the tube, has been demonstrated. A conceptual design has been presented for inspecting tubes up to 7 feet in length in both through-wall and reflection modes. Other results suggest that problems with reverberating sound fields have to be solved before acoustic lenses can be effectively employed to eliminate sound-field focusing in the tube wall during through-wall insonification.

Efforts to examine a butt joint with dye-penetrant, radiographic, and ultrasonic techniques revealed that while holographic interferometry seemed to more clearly identify the presence of a crack-like flaw on or near the inner surface, ultrasonic pulse-echo and pitch-catch techniques at 22 MHz can also indicate the presence of an anomaly. The ultrasonically detected flaw coincided with the holographic result with regard to angular location.

Destructive examination of an overlap tube joint previously scanned with an IR camera revlead that the joint was not bonded uniformly. The region with the best bonding corresponds to a cool spot identified in the IR scan.

Previous Publications Other than Reports

1. W.D. Deininger and D.S. Kupperman, "Infrared Techniques for the Evaluation of Silicon Carbide Heat-exchanger Tubing," Journal of Testing and Evaluation, Vol. 8, No. 1 (January 1980).

2. D.S. Kupperman, N. Lapinski, C. Sciammarella, and D. Yuhas, "Nondestructive Evaluation Techniques for Silicon Carbide Heat-exchanger Tubes," Proceedings of the ARPA/AFML Review of Progress in Quantitative NDE, July 8-13, 1979, La Jolla, CA (to be published).

3. D.S. Kupperman, L. Pahis, D. Yuhas, and T.E. McGraw, "Acoustic Microscopy Techniques for Structural Ceramics," American Ceramic Society Bulletin, Vol. 59, No. 8 (August 1980).

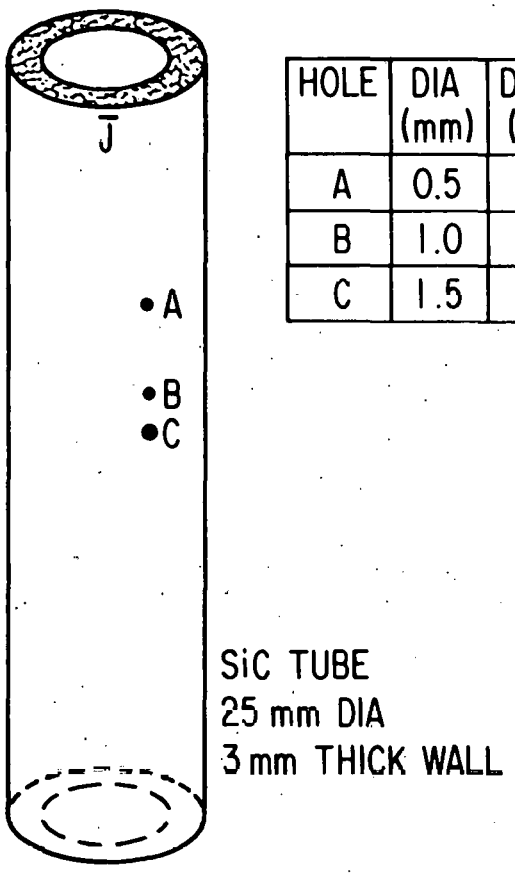

HOLE	DIA (mm)	DEPTH (mm)
A	0.5	0.8
B	1.0	1.5
C	1.5	1.5

Fig. 1. Schematic of SiC Tube with Three Flat-bottom Holes in Outer Wall.

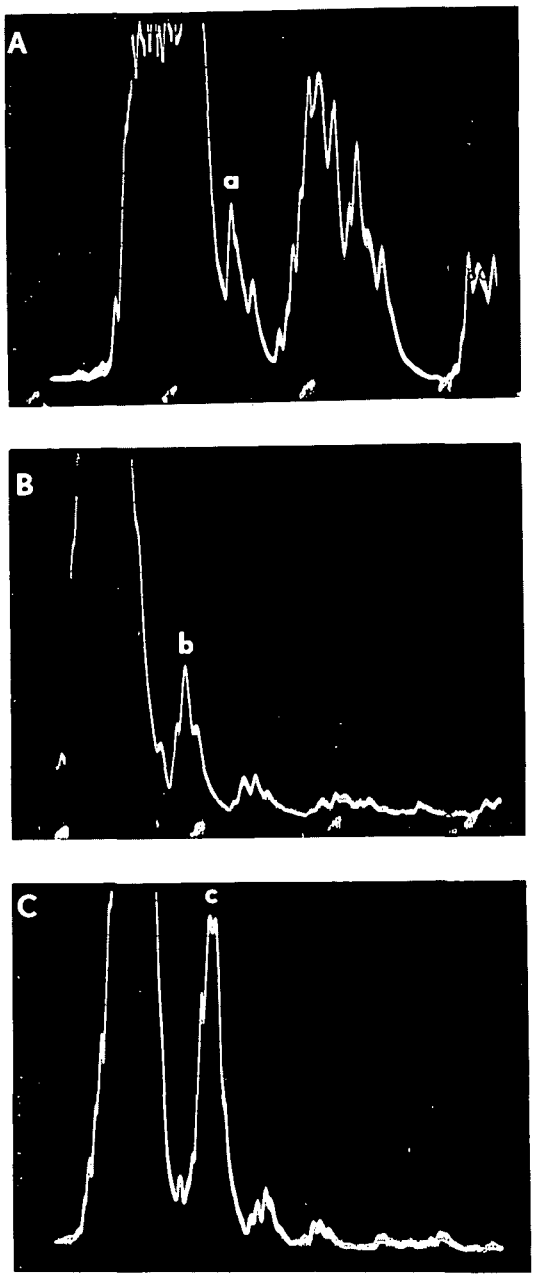

Fig. 2. Ultrasonic Echoes from Flat-bottom Holes Shown in Fig. 1. (a) 0.5 mm dia x 0.8 mm deep; (b) 1.0 mm dia x 1.5 mm deep; (c) 1.5 mm dia x 1.5 mm deep.

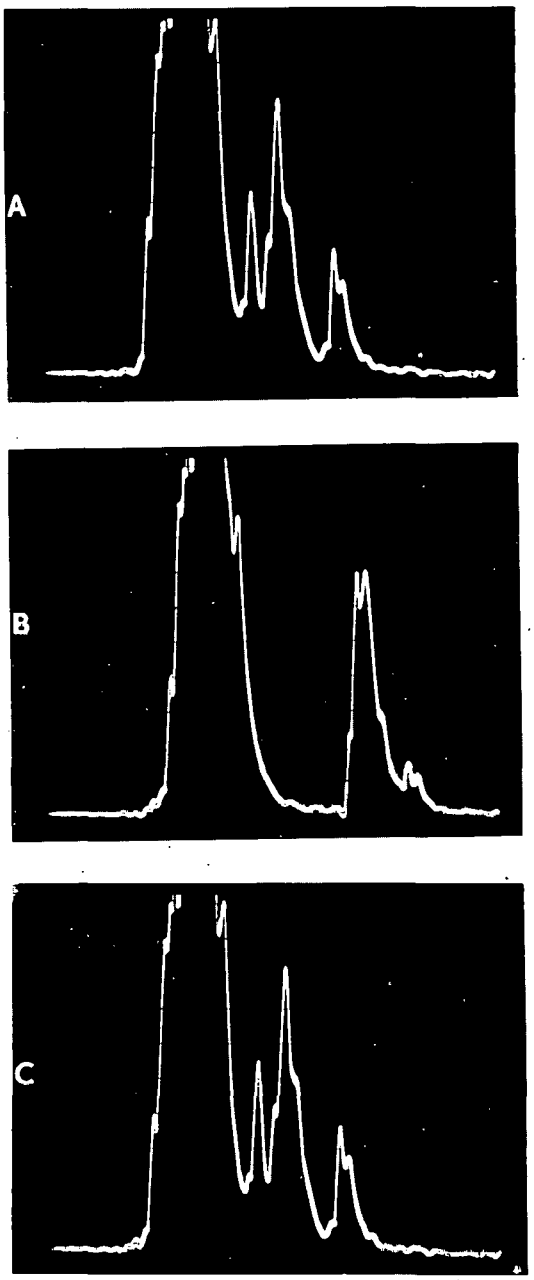

Fig. 3. Ultrasonic Echoes from (a) 1.5-mm-dia Hole, (b) Region of Tube 13 mm Below 1.5-mm-dia Hole, and (c) 1.5-mm-dia Hole After Computer-controlled Traverse Back to Original Position. Traces (a) and (c) are virtually identical.

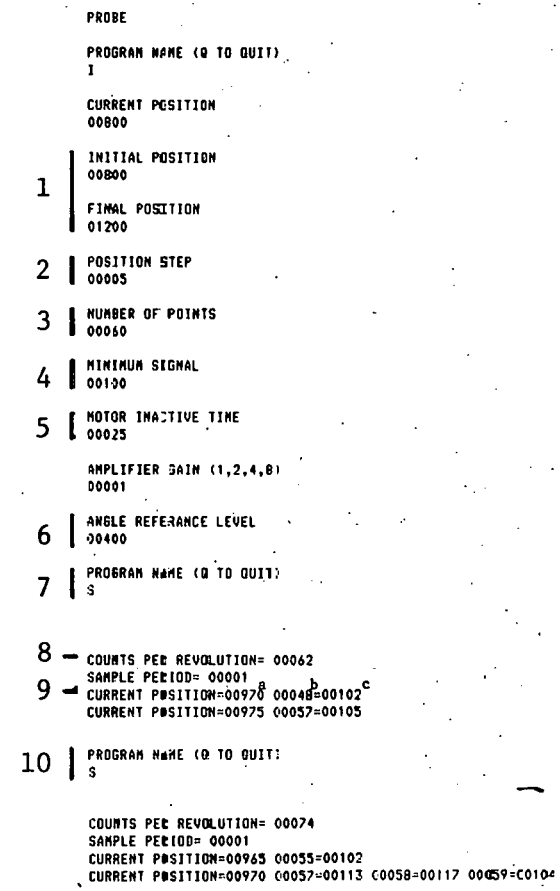

1. Distance of 25 mm between initial and final positions.
2. Tube scanned after every 0.3 mm of axial motion.
3. 60 data points per revolution.
4. A signal with amplitude $\geq$100 units (= 0.25 V of analog output from pulser-receiver) indicates presence of a flaw.
5. 25-ms pause between steps of motor.
6. Signal from support rib provides trigger for marking 0° point of each angular rotation.
7. Start of Scan 1.
8. Time after trigger signal for one rotation of mirror, as calculated by computer (1 count = 3 ms).
9. Axial position (a), angular position (b), and amplitude (c) of first above-threshold signal in Scan 1.
10. Start of Scan 2.

Fig. 4. (Left) Computer Printout of Two Microcomputer-controlled Ultrasonic Scans of SiC Tube J, Indicating Same Notch at Location 970-975 (Scan 1) and 965-970 (Scan 2). (Right) Explanations of Numbered Lines in Printout.

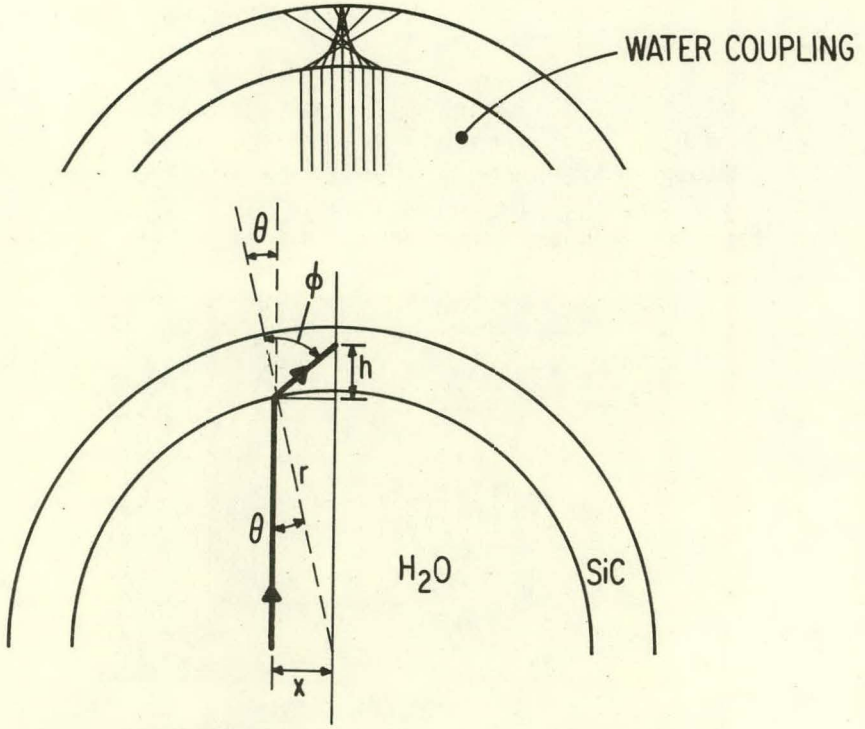

$$h = x/\tan(\phi - \theta)$$

$$h = x/\left\{\tan\left[\arcsin\left(\frac{v_{SiC}\, x}{v_{H_2O}\, r}\right) - \arcsin\left(\frac{x}{r}\right)\right]\right\}$$

Fig. 5. Schematic Showing Refraction (Focusing) of Sound As It Propagates from Inner to Outer Surface of a Water-filled SiC Tube. θ is the insonification angle.

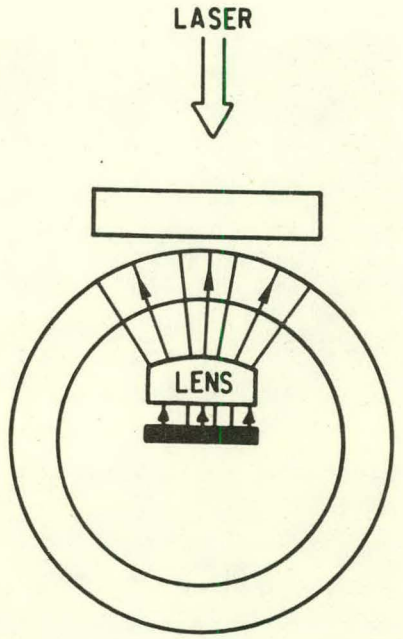

Fig. 6. Schematic Showing the Use of a Diverging Lens to Prevent Sound Focusing Within the Tube Wall.

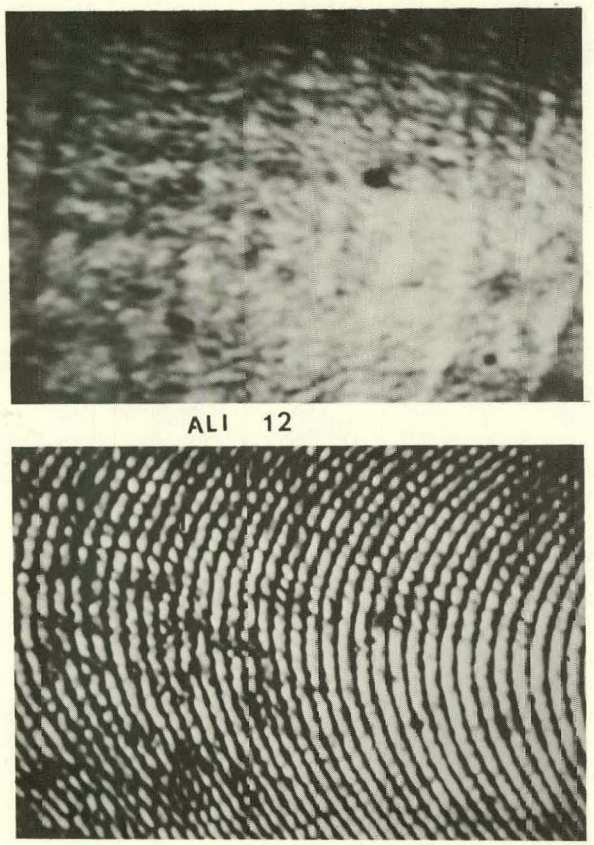

Fig. 7. Acoustic Amplitude Micrograph (Top) and Interferogram of Tube SRI, Showing the Characteristics of a Sound Field Propagated Through an Aluminum Lens with a 10-mm Radius of Curvature.

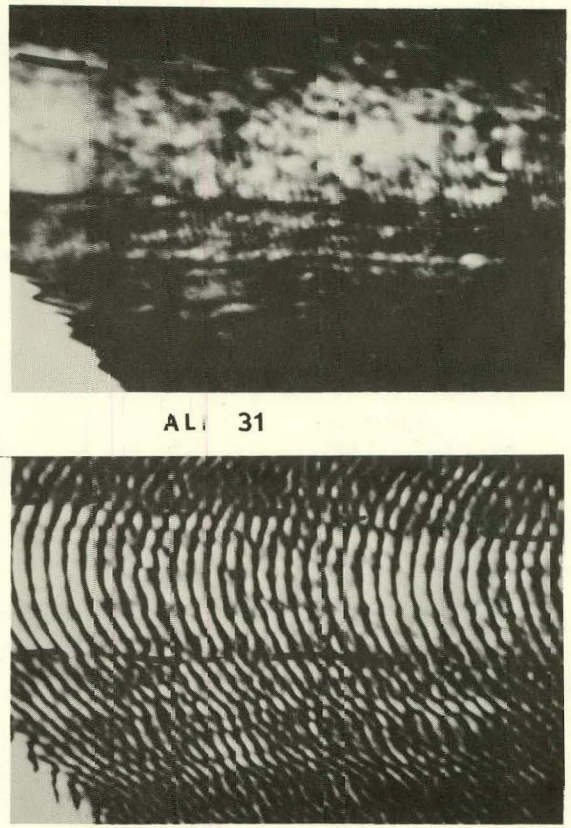

Fig. 8. Acoustic Amplitude Micrograph (Top) and Interferogram of Tube SRI, Showing Typical Image Characteristics Obtained by Through-wall Plane-wave Inscnification of a Tube Segment.

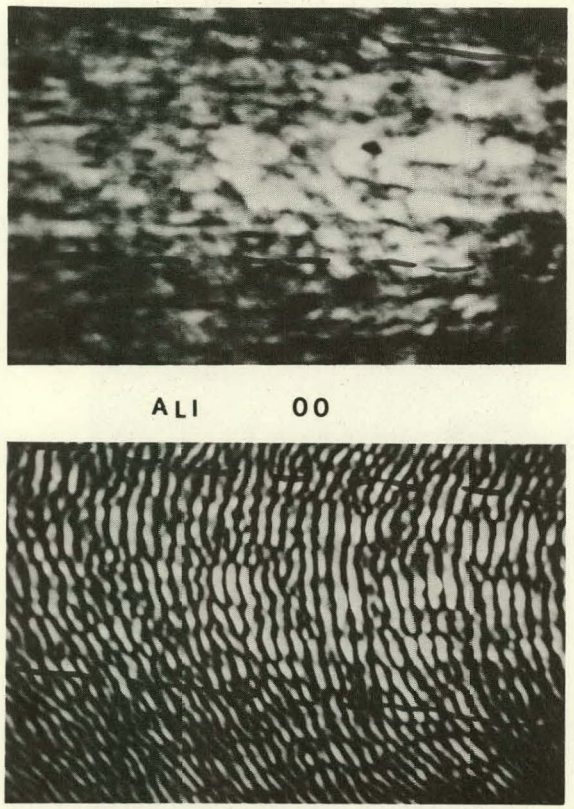

Fig. 9. Acoustic Amplitude Micrograph (Top) and Interferogram of Same Tube Shown in Fig. 8, Obtained by Through-wall Insonification with an Aluminum Lens. Note the increased aperture size and straightening of the fringes compared with Fig. 8.

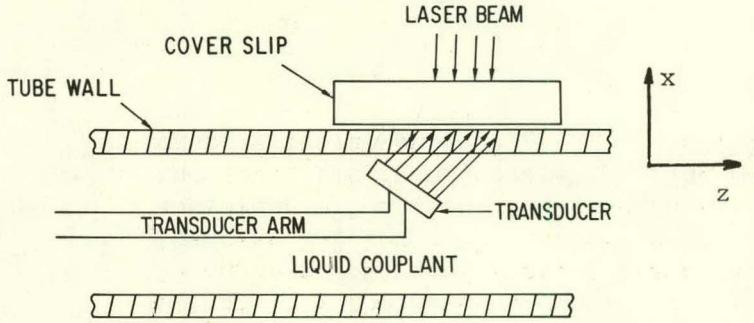

Fig. 10. Insonification Geometry Used to Generate Axially Propagated Through-wall Ultrasonic Waves for Detection by Acoustic Microscopy.

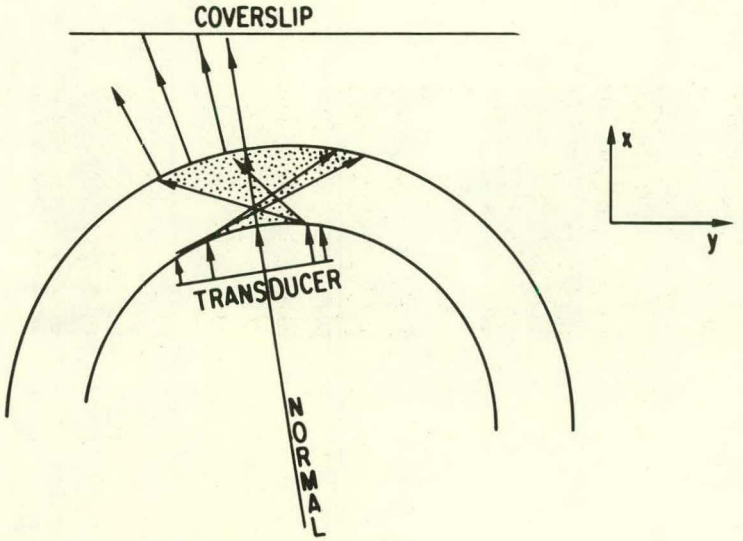

Fig. 11. Insonification Geometry Used to Generate Circumferential Through-wall Ultrasonic Waves for Detection by Acoustic Microscopy. Similar configuration to Fig. 5 (top).

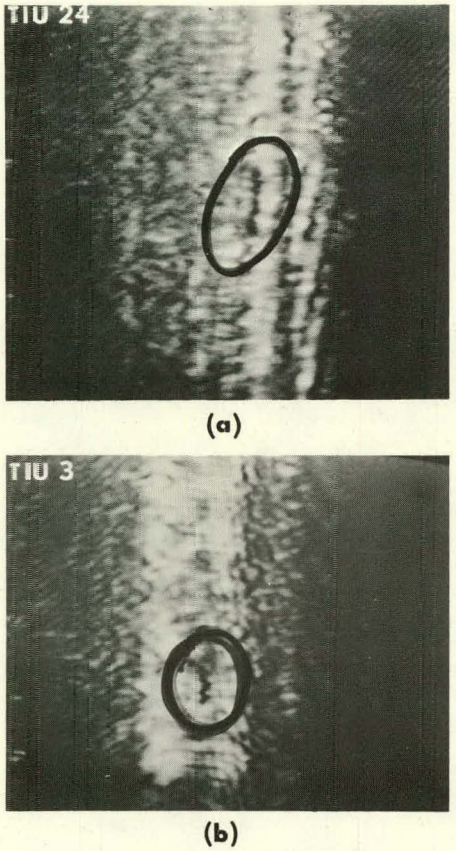

Fig. 12. Acoustic Amplitude Micrographs of Longitudinal EDM Notches (Circled) in the Outer Wall of SiC Tube SRI, Obtained Using Through-wall Circumferential Insonification. Notch dimensions: (a) 1250 μm long x 500 μm deep; (b) 250 μm long x 125 μm deep.

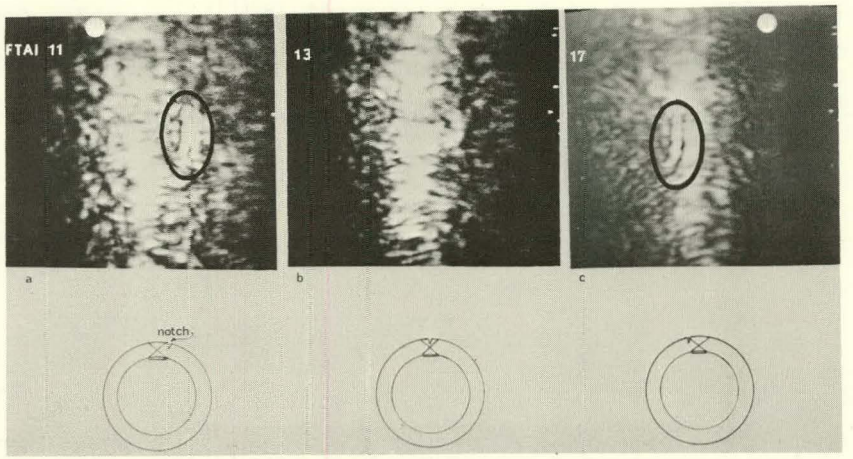

Fig. 13. Acoustic Amplitude Micrographs Taken in the Vicinity of the Notch Shown in Fig. 12a, with Through-wall Circumferential Insonification. The sketch below each micrograph shows the approximate location of the notch relative to the sound field and coverslip. The notch is visible in (a) and (c), but not in (b).

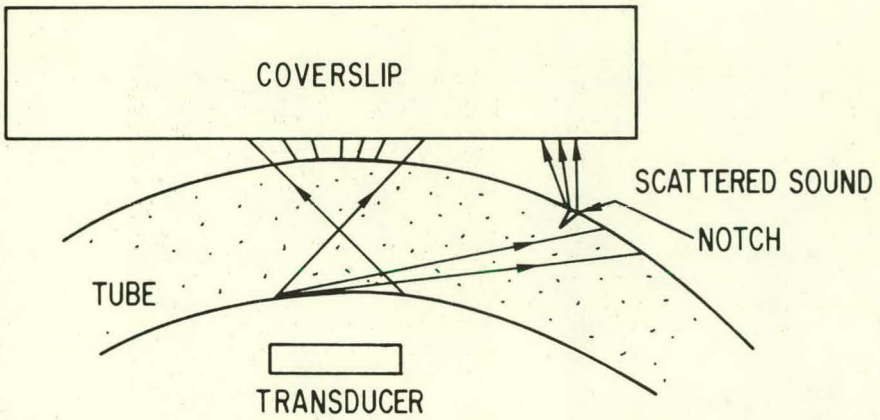

Fig. 14. Schematic Illustrating the Geometry and Principles of Acoustic Dark-field Imaging.

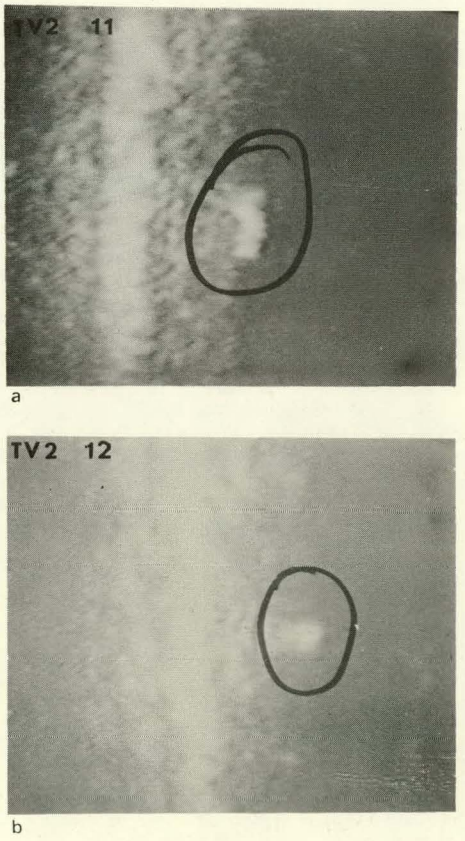

Fig. 15. Dark-field Images of Same Notches Shown in Fig. 12.

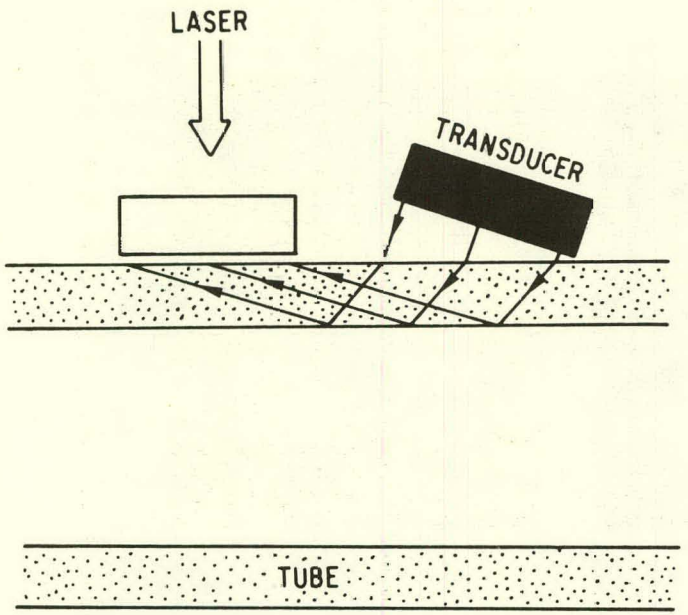

Fig. 16. Schematic Showing External Axial Insonification.

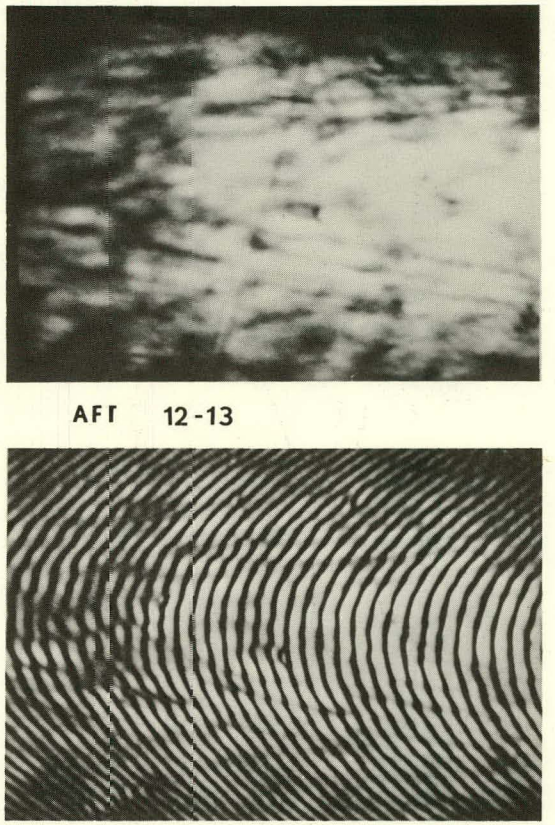

Fig. 17. Acoustic Amplitude Micrograph (top) and Interferogram of "Clean" Zone in Tube SRI, Obtained with External Axial Insonification.

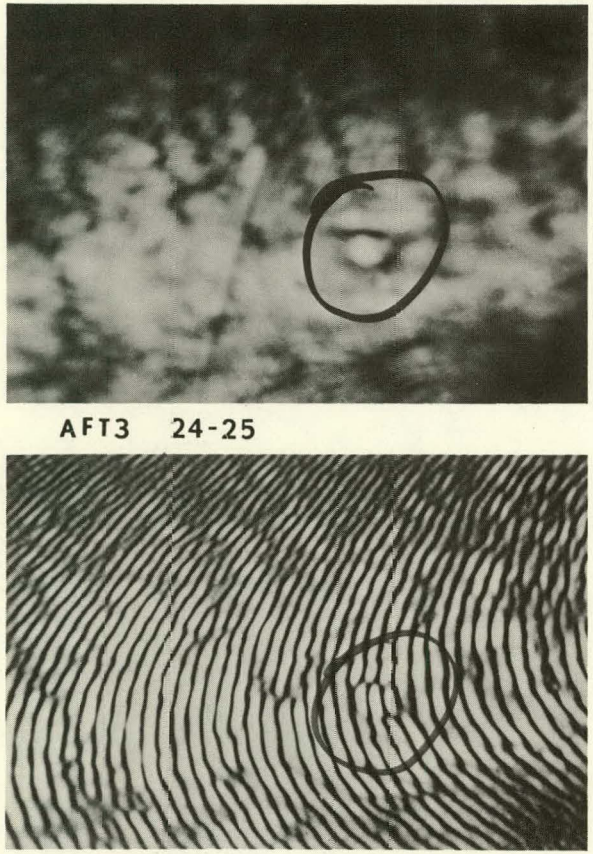

Fig. 18. Acoustic Amplitude Micrograph (Top) and Interferogram of Buried Inclusion (Circled) in Tube SRI, Obtained with External Axial Insonification.

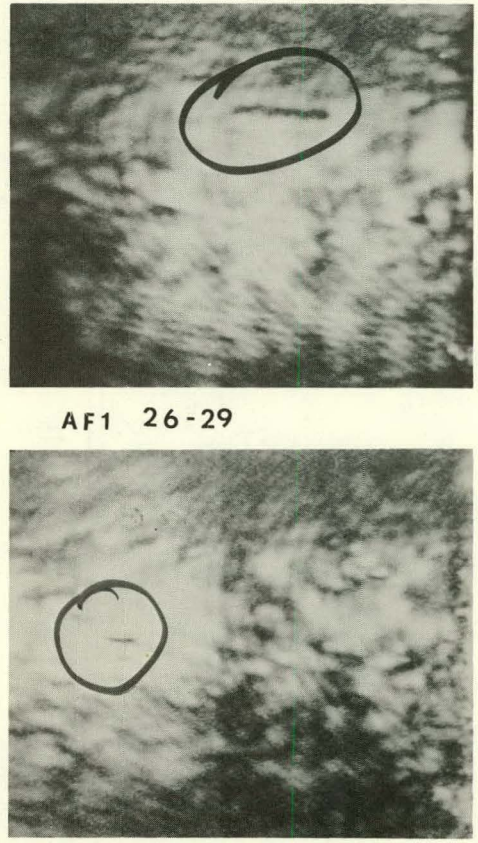

Fig. 19. Acoustic Amplitude Micrographs of the Two Longitudinal Notches Shown in Fig. 12, Obtained with External Axial Insonification.

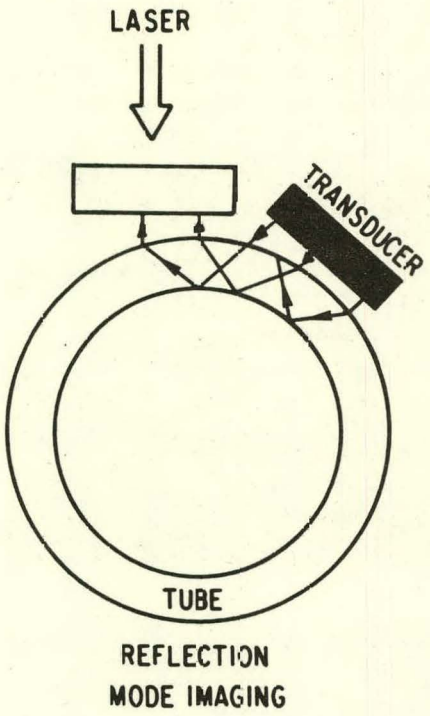

Fig. 20. Schematic Showing External Circumferential Insonification.

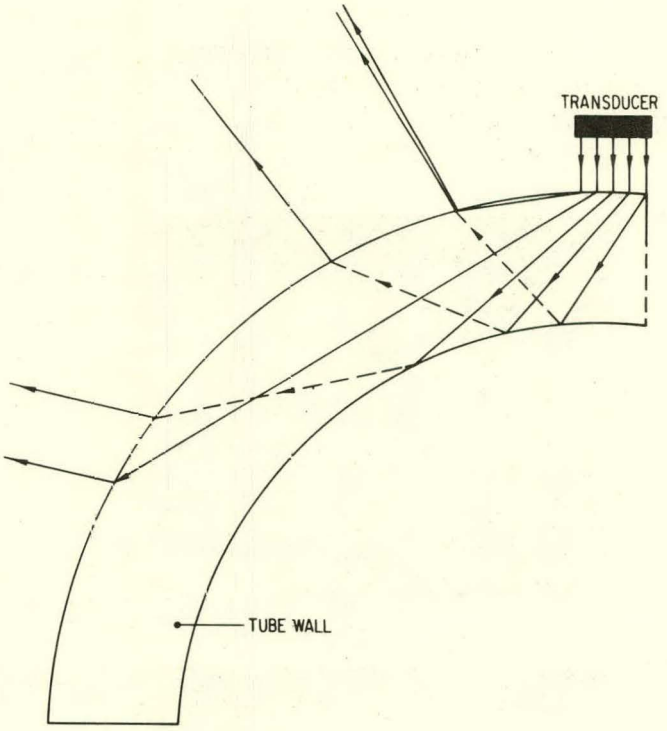

Fig. 21. Ray-tracing Diagram Showing Propagation of Shear Waves in a Tube Undergoing External Circumferential Insonification.

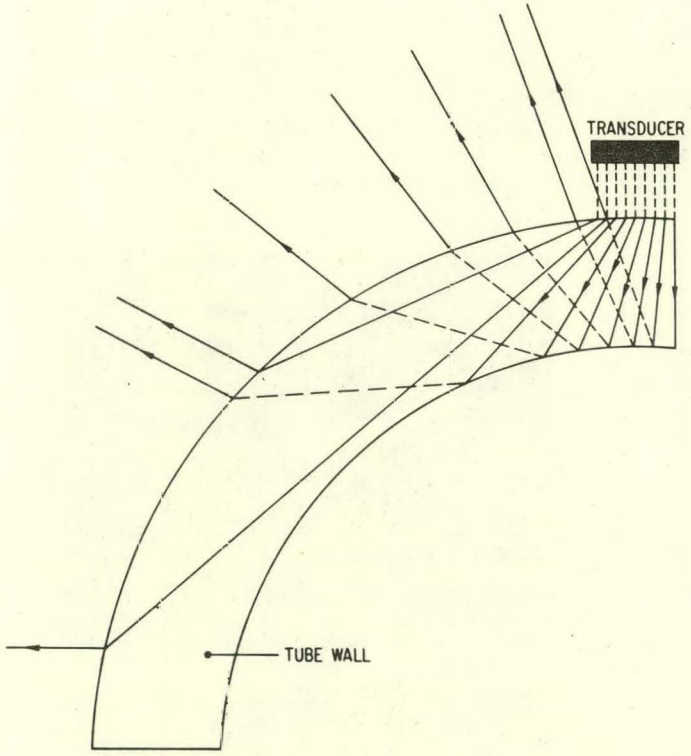

Fig. 22. Ray-tracing Diagram Showing Propagation of Longitudinal Waves in a Tube Undergoing External Circumferential Insonification.

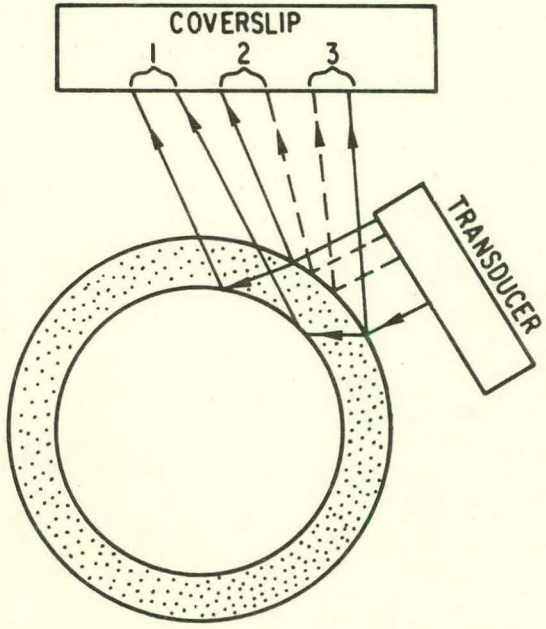

Fig. 23. Schematic Showing the Approximate Locations of the Three Sound Fields Created by External Circumferential Insonification.

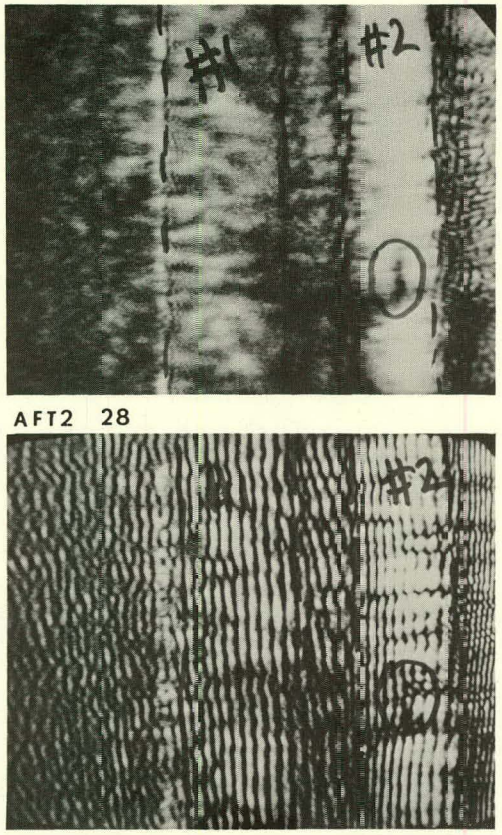

Fig. 24. Acoustic Amplitude Micrograph (Top) and Interferogram of Tube SRI with External Circumferential Insonification. Image of EDM notch is circled. Numbers on micrographs refer to sound fields defined in Fig. 23.

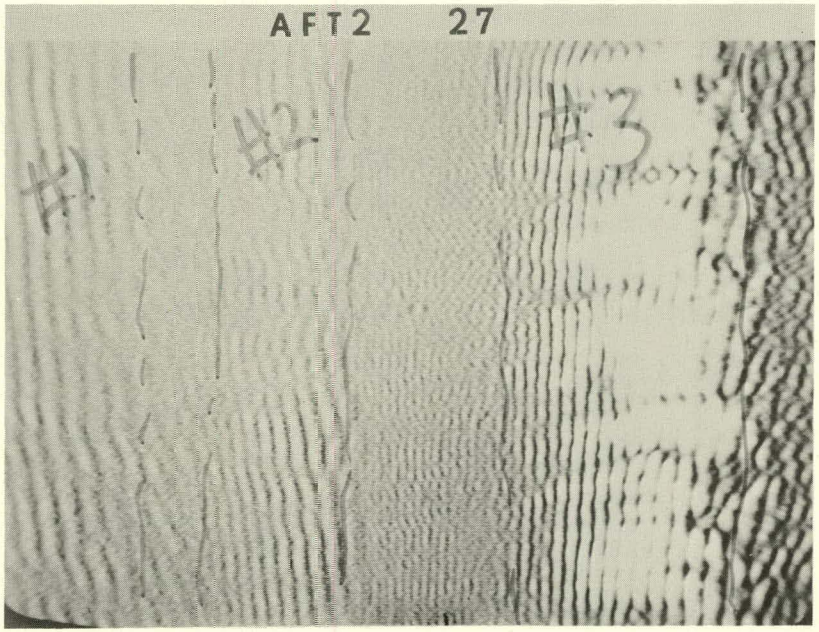

Fig. 25. Interferogram Produced by External Circumferential Insonification. Numbers refer to sound fields defined in Fig. 23.

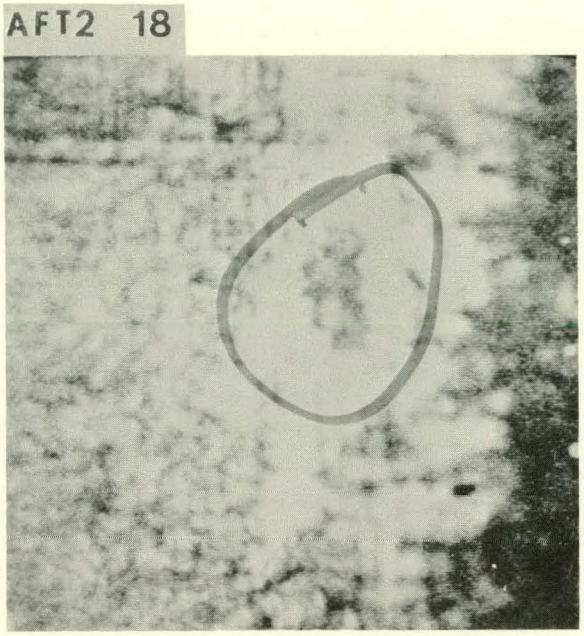

Fig. 26. Acoustic Amplitude Micrograph Produced Using External Circumferential Insonification, Showing Longitudinal EDM Notch (Circled).

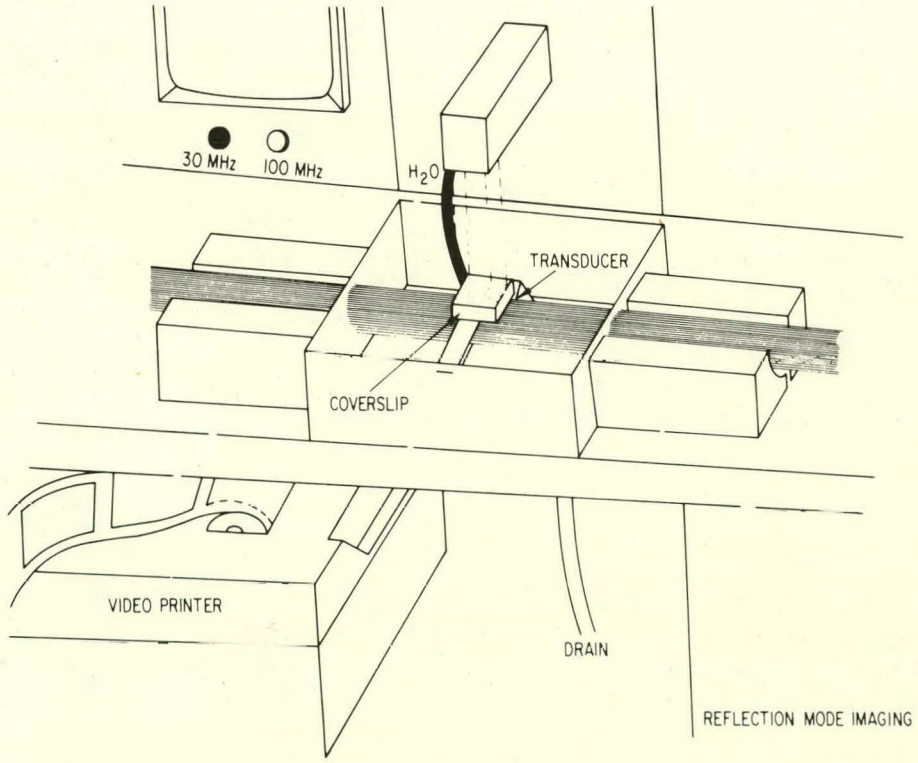

Fig. 27. Schematic of Tube Scanner Operating in Reflection Mode.

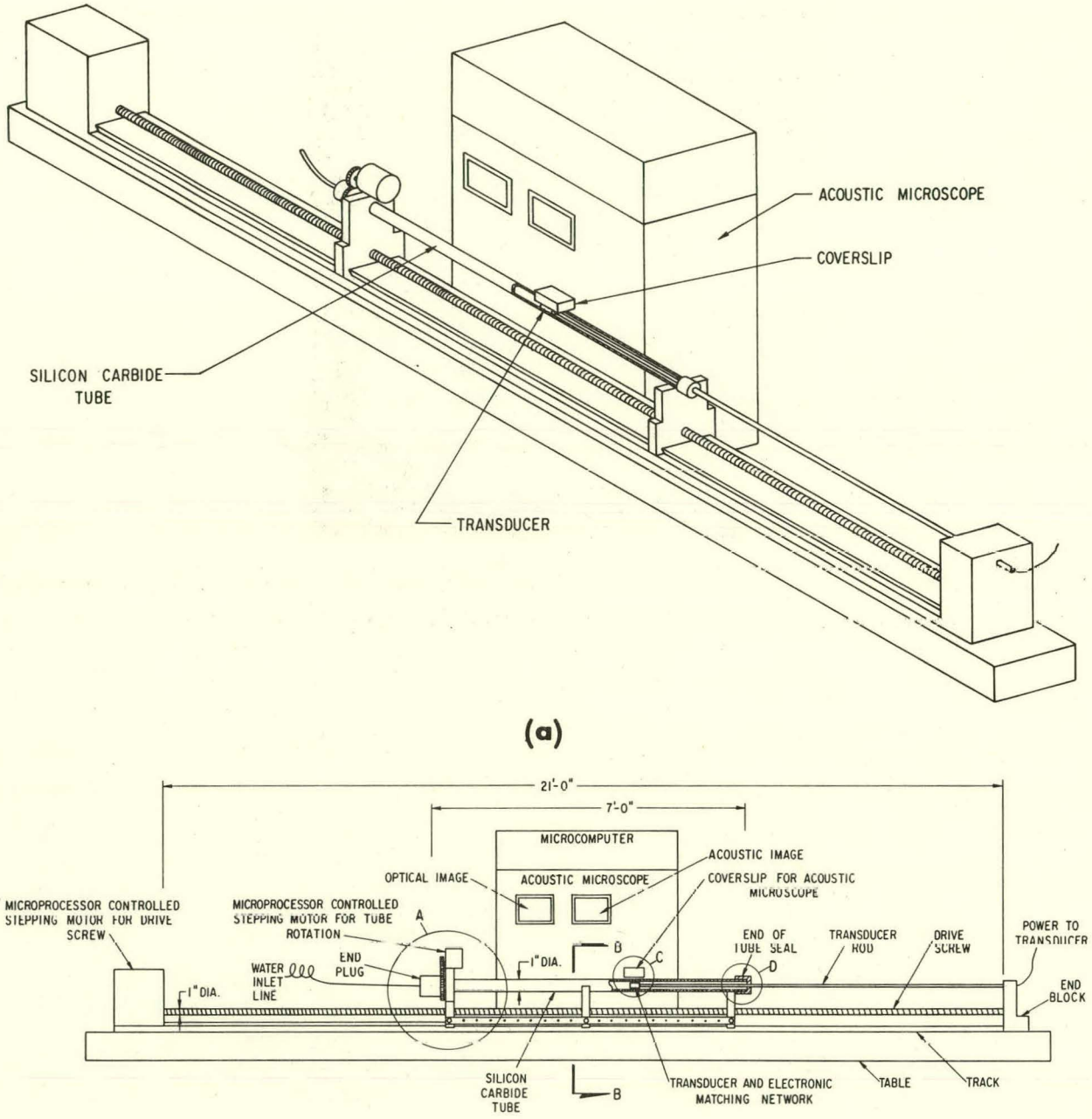

Fig. 28. Conceptual Design for Through-transmission Acoustic Microscopy of Long SiC Tubes. (a) Isometric view; (b) schematic of overall system; (c) details of regions A, B, C, D of (b).

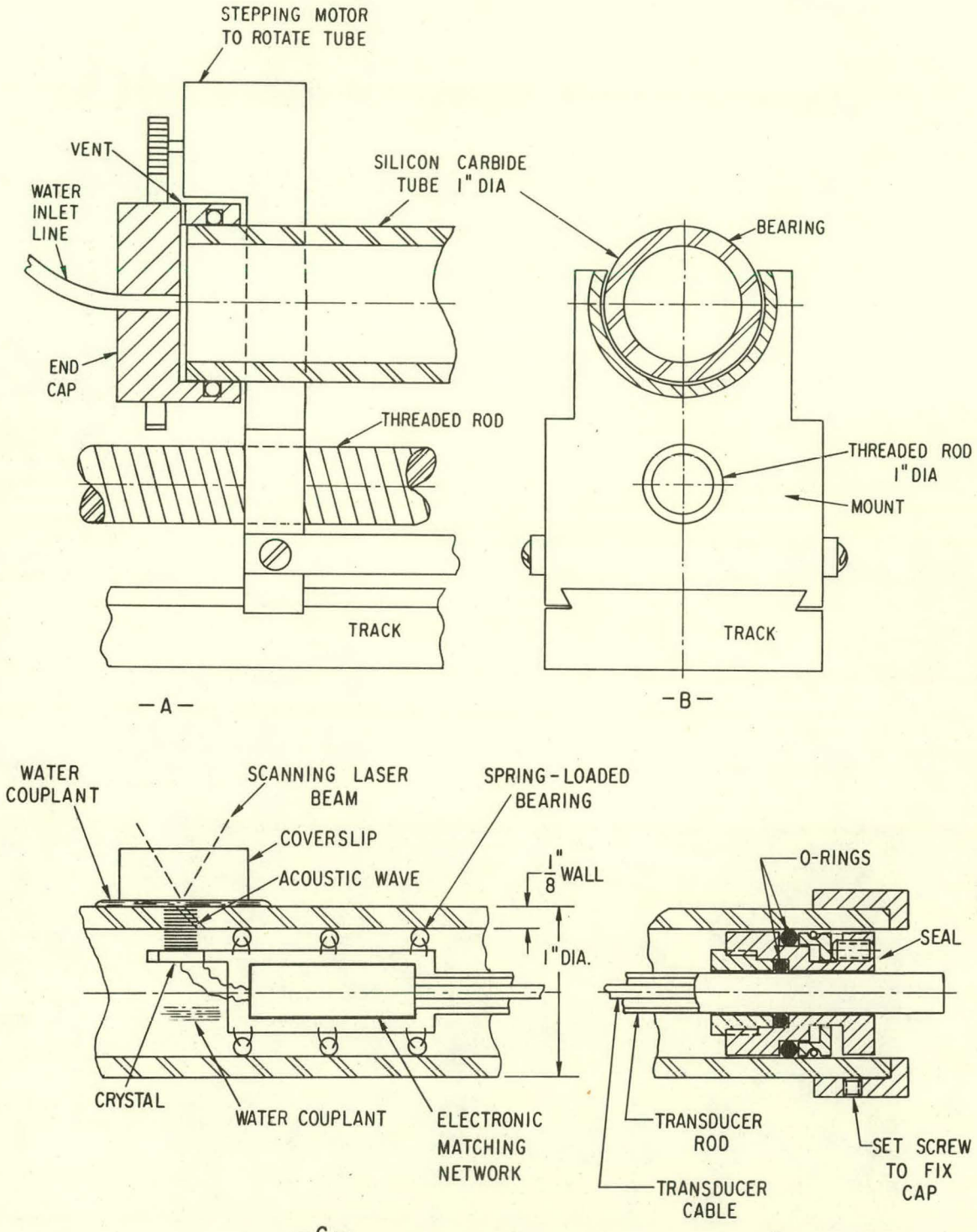

(c)

Fig. 28 (contd.)

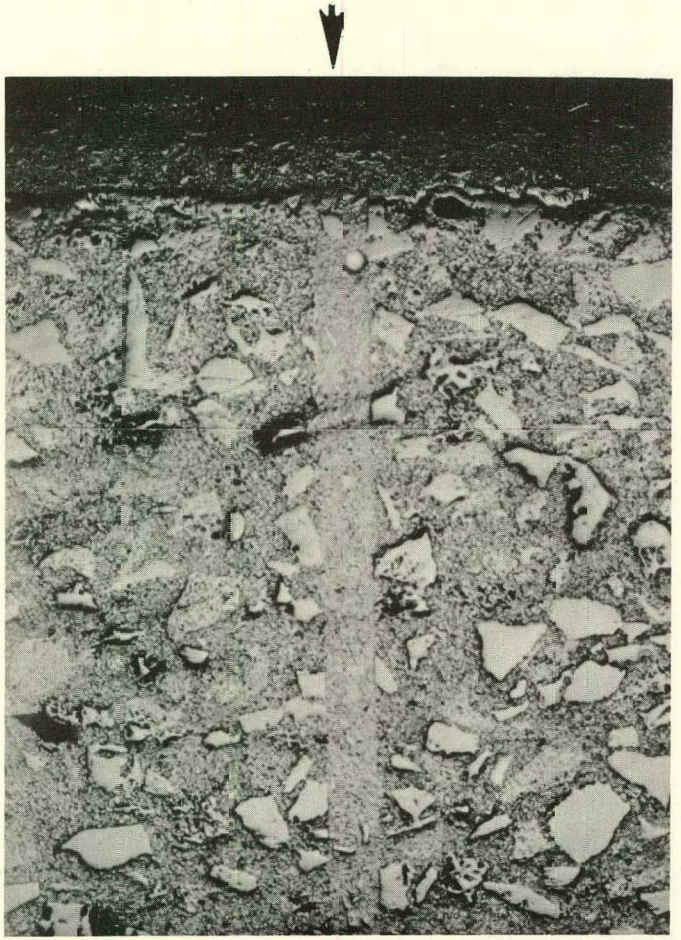

Fig. 29. Section of SiC Tube NC430-J7, Showing ∿150-μm-Wide Ceramic Butt Joint (Arrow). Outer surface of tube is at top of micrograph. Small grain size of joint relative to tube wall is evident.

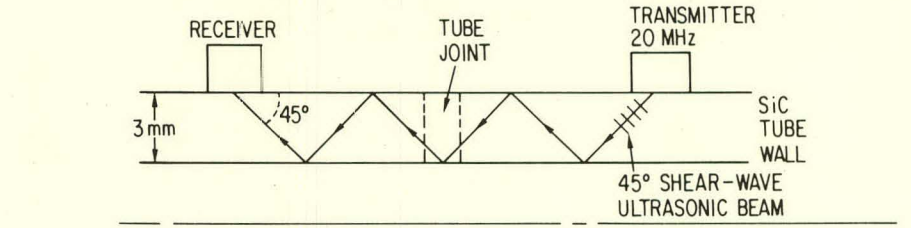

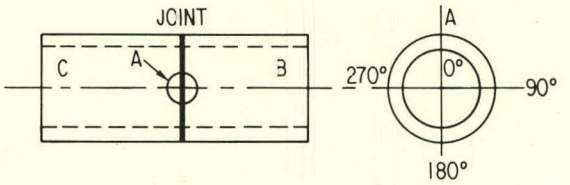

RELATIVE AMPLITUDE OF RECEIVED ULTRASONIC SIGNAL

TUBE REGION	ANGULAR POSITION			
	0°	90°	180°	270°
A (JOINT)	40	90	90	100
B	70	–	–	–
C	70	–	–	–

Fig. 30. (Top) Schematic of Arrangement Used for Ultrasonic Inspection of SiC Tube Joint, Using Two 20-MHz Transducers in a Pitch-Catch Mode; (Bottom) Inspection Results. The reduced signal amplitude at A-0° indicates an anomaly in this region.

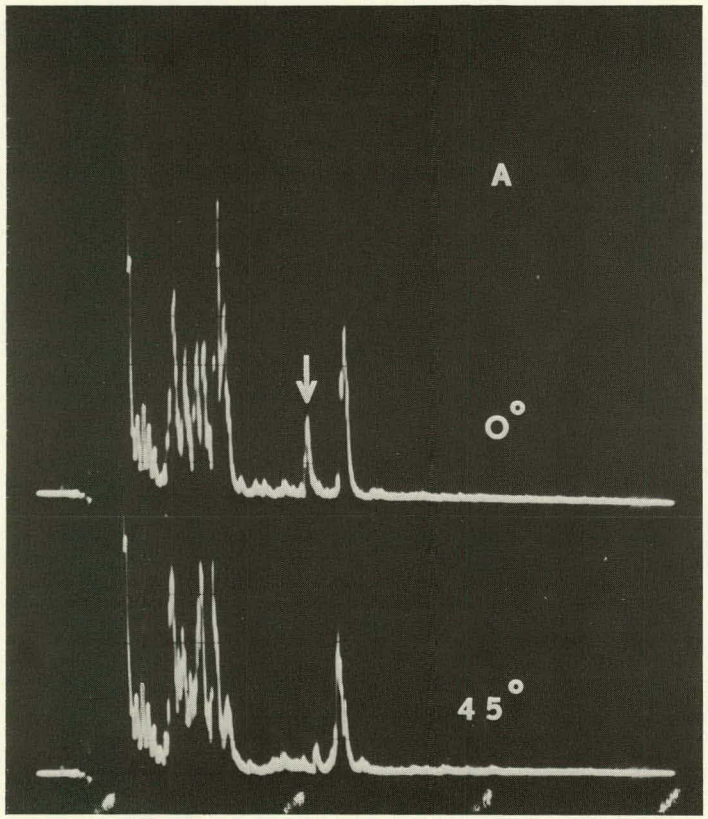

Fig. 31. "A-scan" Traces Obtained at 0° and 45° Positions of Region A (Joint) in Tube J6. An anomaly (arrow) is indicated in the 0° scan. No anomalies were detected at 45° or other circumferential positions within Region A. The present result agrees with those obtained[9,11] by ultrasonic through-transmission and holographic techniques.

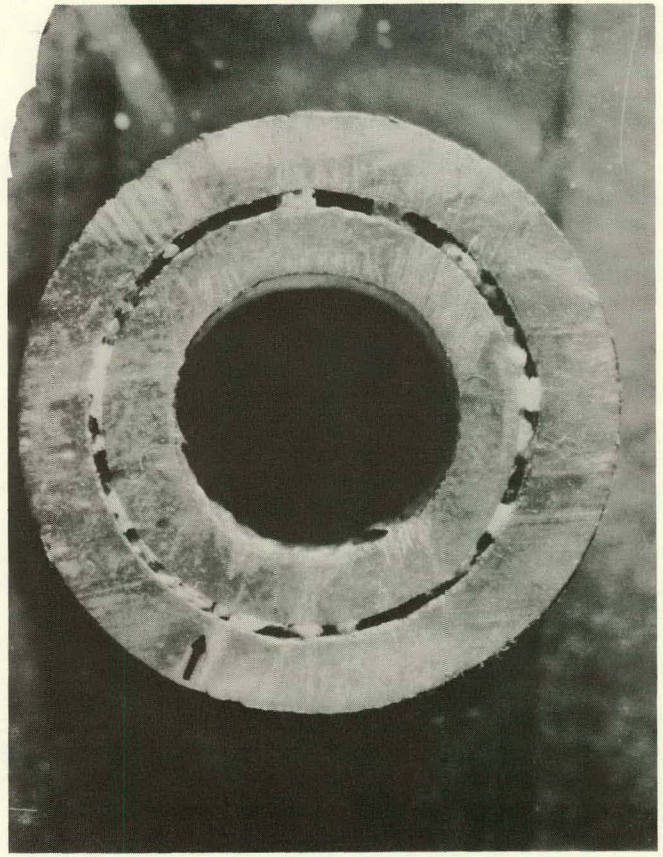

Fig. 32. Cross Section of Overlap Joint Showing Area (Arrow) with Better Bonding Than in the Rest of the Joint. An infrared scan[10] had previously shown better heat transfer in this region.

REFERENCES

1. F.F. Lange, Structural Ceramic Materials Under Development, Gas Turbine Conference and Products Show, Houston, TX, March 2-6, 1975, paper 75-GT-107.

2. A.G. Evans, G.S. Kino, P.T. Kuri-Yakub and B.R. Tittman, Failure Prediction in Structural Ceramics, Material Eval. 35 (4), 85 (April 1977).

3. A.J. Bahr, Microwave Techniques for Nondestructive Evaluation of Ceramics, Final Report AMMRC-CTR-77-29, SRI International, Menlo Park, CA (Nov. 1977).

4. P.T. Kuri-Yakub, Acoustic Surface Wave Scattering: The Detection of Surface Cracks in Ceramics, Report SC5064-2TR, Rockwell International Science Center, Thousand Oaks, CA (Dec. 1977).

5. Y.H. Wong and R.L. Thomas, Laser Photoacoustic Techniques for NDE, presented at ARPA/AFML Review of Progress in Quantitative NDE, Scripps Institution of Oceanography, La Jolla, CA (July 12-21, 1978).

6. A.G. Evans and M. Linzer, Failure Prediction in Structural Ceramics Using Acoustic Emission, J. Am. Ceram. Soc. 56 (11), 575 (1973).

7. J.E. Ritter, Proof Testing of Ceramics, 81st Annual Meeting of the American Ceramic Society, Cincinnati, OH, April 29-May 2, 1979, paper 14-SC-79.

8. D.S. Kupperman, C. Sciammarella, N.P. Lapinski, A. Sather, D. Yuhas, L. Kessler, and N.F. Fiore, Preliminary Evaluation of Several NDE Techniques for Silicon Nitride Gas-Turbine Rotors, Argonne National Laboratory Report ANL-77-89 (Jan. 1978).

9. D.S. Kupperman, D. Yuhas, W. Deininger, and C. Sciammarella, Nondestructive Evaluation Techniques for Silicon Carbide Heat-exchanger Tubes, Second Annual Report, October 1978-June 1979, Argonne National Laboratory Report ANL-79-103 (November 1979).

10. D.S. Kupperman, D. Yuhas, and M.J. Caines, Development of Nondestructive Evaluation Techniques for High-temperature Ceramic Heat Exchanger Components, Tenth Quarterly Report, January-March 1980, Argonne National Laboratory Report ANL/MSD/FE-80-2 (April 1980).

11. D.S. Kupperman, C. Sciammarella, M.J. Caines, and M. McNeela, Nondestructive Evaluation Techniques for Silicon Carbide Heat-exchanger Components, Eleventh Quarterly Report, April-June 1980, Argonne National Laboratory Report ANL/MSD/FE-80-4 (August 1980).

Distribution for ANL/MSD/FE-80-7

Internal:

B. R. T. Frost
J. J. Roberts
R. W. Weeks
A. A. Jonke (10)
E. L. Carls
M. J. Caines
E. M. Stefanski (4)
W. A. Ellingson (2)
K. J. Reimann
C. A. Youngdahl
C. R. Kennedy
D. R. Diercks
E. L. Hartig
D. S. Kupperman (20)
R. B. Poeppel
R. Arons
A. B. Krisciunas
ANL Contract File
ANL Libraries
TIS Files (6)

External:

DOE-TIC (27)
Manager, Chicago Operations and Regional Office, DOE
Chief, Office of Patent Counsel, DOE-CORO
President, Argonne Universities Association
Materials Science Division Review Committee:
- E. A. Aitken, General Electric Co., Sunnyvale
- G. S. Ansell, Rensselaer Polytechnic Inst.
- A. Arrott, Simon Fraser U.
- R. W. Balluffi, Massachusetts Inst. Technology
- S. L. Cooper, U. Wisconsin-Madison
- C. Laird, U. Pennsylvania
- M. E. Shank, Pratt & Whitney, East Hartford
- C. T. Tomizuka, U. Arizona
- A. R. C. Westwood, Martin Marietta Labs.

U. S. Department of Energy, Washington:
- J. M. Bartis
- J. Batchelor
- S. J. Dapkunas
- G. Dick
- L. C. Ianniello
- T. K. Lau
- E. A. Lloyd
- L. Miller
- J. L. Powell
- I. Wender
- K. Youseff

DOE Grand Forks Energy Technology Center:
- G. Baker
- M. W. Heher

DOE Idaho Operations Office:
- W. H. Thielbahr

DOE Laramie Energy Technology Center:
- C. F. Brandenburg

DOE Morgantown Energy Technology Center:
- D. Freeburn
- G. Friggens
- R. L. Gall
- J. F. Gardner
- J. Halow
- J. M. Hobday

R. Lewis
J. Notestein
K. Pater
A. A. Pitrolo
W. E. Wallace

DOE Pittsburgh Energy Technology Center:

D. Dubis
J. D. Hickerson
A. G. Sharkey, Jr.

Air Force Materials Lab., Dayton:

R. L. Crane
H. Graham

Army Materials and Mechanics Research Center, Watertown:

R. Brockelman
A. Broz
R. Katz
E. Lenoe

NASA Lewis Research Center:

S. Klima

National Bureau of Standards, Washington:

H. S. Berger
E. Fuller

Oak Ridge National Laboratory:

R. A. Bradley
R. McClung
V. J. Tennery

Other Government - University - Industry:

N. Ault, Norton Co., Worcester, Mass.
A. J. Bahr, Stanford Research Inst.
J. E. Bigger, Electric Power Research Inst.
A. Borkmanis, Harrison Radiator, Lockport, N. Y.
D. Cassidy, Ford Motor Co., Dearborn, Mich.
T. Coyle, Solar Energy Research Inst.
W. Deininger, Ft. Collins, Colo.
N. F. Fiore, U. Notre Dame
S. C. Gambrell, U. Alabama
L. Kessler, Sonoscan, Inc., Bensenville, Ill.
P. Khandelwal, Detroit Diesel Allison, Indianapolis
B. T. Khuri-Yakub, Stanford U.
G. Kino, Stanford U.
D. Kotchik, Garrett-AiResearch, Torrance, Calif.
F. F. Lange, Rockwell Science Center, Thousand Oaks, Calif.
H. W. Larisch, Coors Porcelain Co., Golden, Colo.
D. C. Larsen, IIT Research Inst., Chicago
W. Meier, Coors Porcelain Co., Golden, Colo.
A. B. Metcalfe, Solar Turbines International, San Diego
I. Most, Hague International, S. Portland, Me.
V. L. Newhouse, Purdue U.
G. T. Peters, United Technologies Research Center, East Hartford
A. Pietsch, AiResearch Manufacturing Co., Phoenix
C. W. Robertson, E. I. duPont de Nemours & Co., Wilmington
D. Rose, U. S. Army TARADCOM, Warren, Mich.
R. D. Roy, Ontario Research Foundation, Mississauga, Ont., Canada
J. Schuldies, AiResearch Manufacturing Co., Phoenix

C. Sciammarella, Illinois Inst. of Technology, Chicago
R. Springer, Materials Technology Corp., Dallas
M. Srinivasan, Carborundum Co., Niagara Falls
M. Stevens, IBM Corp., Poughkeepsie
J. Stringer, Electric Power Research Inst.
M. E. Ward, International Harvester, Solar Div., San Diego
R. Y. Wong, Bell Telephone Labs., Murray Hill
D. Yuhas, Sonoscan, Inc., Bensenville, Ill.